Matrix Biology Plus 24 (2024) 100164

Contents lists available at ScienceDirect

Matrix Biology Plus

journal homepage: www.sciencedirect.com/journal/matrix-biology-plus

# A human stem cell-derived model reveals pathologic extracellular matrix remodeling in diabetic podocyte injury

Yasmin Roye [a], Carmen Miller [b], Titilola D. Kalejaiye [a,1], Samira Musah [a,c,d,e,f,g,*]

[a] Department of Biomedical Engineering, Pratt School of Engineering, Duke University, Durham, NC, USA
[b] Department of Biology, Trinity College of Arts and Sciences, Duke University, Durham NC, USA
[c] Department of Medicine, Division of Nephrology, Duke University School of Medicine, Durham, NC, USA
[d] Department of Cell Biology, Duke University School of Medicine, Durham, NC, USA
[e] Center for Biomolecular and Tissue Engineering, Duke University, Durham, NC, USA
[f] Affiliate Faculty of the Developmental and Stem Cell Biology Program, Duke University School of Medicine, Durham, NC, USA
[g] MEDx Investigator, Duke University, Durham, NC, USA

ARTICLE INFO

*Keywords:*
Diabetic nephropathy
Human induced pluripotent stem cells
Podocytes
Hyperglycemia
Collagen (IV)
Decellularized extracellular matrix

ABSTRACT

Diabetic nephropathy results from chronic (or uncontrolled) hyperglycemia and is the leading cause of kidney failure. The kidney's glomerular podocytes are highly susceptible to diabetic injury and subsequent non-reversible degeneration. We generated a human induced pluripotent stem (iPS) cell-derived model of diabetic podocytopathy to investigate disease pathogenesis and progression. The model recapitulated hallmarks of podocytopathy that precede proteinuria including retraction of foot processes and podocytopenia (detachment from the extracellular matrix (ECM)). Moreover, hyperglycemia-induced injury to podocytes exacerbated remodeling of the ECM. Specifically, mature podocytes aberrantly increased expression and excessively deposited collagen (IV)α1α1α2 that is normally abundant in the embryonic glomerulus. This collagen (IV) imbalance coincided with dysregulation of lineage-specific proteins, structural abnormalities of the ECM, and podocytopenia – a mechanism not shared with endothelium and is distinct from drug-induced injury. Intriguingly, repopulation of hyperglycemia-injured podocytes on decellularized ECM scaffolds isolated from healthy podocytes attenuated the loss of synaptopodin (a mechanosensitive protein associated with podocyte health). These results demonstrate that human iPS cell-derived podocytes can facilitate *in vitro* studies to uncover the mechanisms of chronic hyperglycemia and ECM remodeling and guide disease target identification.

## Introduction

Diabetic nephropathy (DN) advances to end-stage kidney disease (ESKD) more often than any other kidney disease comorbidity [1]. Despite advances in the use of anti-hypertensive and anti-hyperglycemic drugs to help manage kidney disease, DN is still an irreversible disease and the prevalence of ESKD is expected to increase [2–4]. ESKD is clinically managed with dialysis (~70 %) or organ transplantation (~30 %) [4], but affected patients experience dramatically shortened life span and reduced quality of life [5,6]. Understanding the causes, as well as the cellular and molecular basis of DN, can guide therapeutic development to halt progression of the disease or restore kidney function in the future.

Kidney tissue repair or regeneration following DN has been challenging partly due to the intricate nature of the nephron including the glomerulus. The glomerular filtration barrier selectively filters molecules through a 3-component capillary wall consisting of vascular endothelium, a glomerular basement membrane (GBM), and the highly specialized, post-mitotic visceral epithelium called podocytes, which are highly sensitive to diabetic perturbations and lack regenerative capacity. Uncontrolled hyperglycemia damages podocytes through processes that include increased release and paracrine signaling of pro-inflammatory molecules from the microvasculature, particularly IL-6 and TNFα [7,8], which result in changes to the podocyte cytoarchitecture and phenotype. Particularly, diabetes perturbs podocyte foot processes – the primary and secondary projections that extend from the cell's body and whose function is to wrap around the microvasculature and interdigitate between neighboring podocytes to form the slit

* Corresponding author.
*E-mail address:* samira.musah@duke.edu (S. Musah).
[1] Current affiliation: Department of Cell Biology, Duke University, Durham NC, USA.

https://doi.org/10.1016/j.mbplus.2024.100164
Received 4 July 2024; Received in revised form 16 October 2024; Accepted 27 October 2024
Available online 2 November 2024

diaphragm [9–11]. In affected patients, diabetic podocytopathy is clinically characterized by the widening/flattening of foot processes (effacement), cellular hypertrophy, and ultimately podocyte detachment from the GBM (podocytopenia) that leads to proteinuria [12,13]. Inter-species differences have slowed translation of preclinical findings from *in vivo* animal models to humans [14,15], which limits our understanding of the manifestations and mechanisms of podocytopenia. Emergent models derived from stem cells can help bridge the gap between animal models and human patients by providing physiologically relevant platforms that are more faithful to the donor's biology.

In this study, we employed a human iPS cell-derived model of diabetic podocytopathy to unveil compositional and structural changes at the cell-ECM interface related to podocytopenia. Our stem cell differentiation method has already been validated and replicated across institutions and independent research labs and used successfully in multiple contexts within industrial- and academic settings. Furthermore, multiple published research studies using the established human iPS cell-derived podocyte differentiation method employed in this study have showcased the robustness of the system and provided valuable insights on pertinent topics such as SARS-CoV-2 infectivity in glomerular podocytes, modulation of the YAP-TEAD axis in podocyte injury, biomimetic membranes to induce tissue-specific endothelium through tissue-tissue interfacing with podocytes, and the use of CRISPR/Cas9 genome editing to uncover the genetic basis of podocyte development and disease phenotype[16–20]. Using this established podocyte differentiation strategy, we also examined whether ECM from "healthy" podocytes could serve as supportive platforms to attenuate injury phenotypes. It is well-established that podocytes are the primary producers of collagen (IV)α3α4α5 in the mature kidney glomerulus, which is a heterotrimer that represents 50 % of the GBM [21]. Collagen (IV) homeostasis has been implicated in glomerular development and disease; at the capillary loop stage of nephrogenesis, podocytes turn over production of the embryonic isoform, collagen (IV)α1α1α2, to the mature isoform, collagen (IV)α3α4α5, to mediate the fusion of the GBM [22–24]. When podocytes fail to produce the mature collagen (IV) isoform, the basement membrane stalls in the developmental or immature stage, which can lead to compensatory mechanisms including excessive or aberrant expression of the embryonic isoform. An abundance of the embryonic isoform is deleterious to glomerular integrity partly due to increased susceptibility to degradation by matrix metalloproteinases (MMPs) which has been documented in Alport Syndrome (a genetic form of kidney disease resulting from the absence of collagen (IV)α3α4α5)[25]. When GBM assembly is compromised in this way, it hinders proper association or integration of other basement membrane molecules, such as the mature isoform of laminin-11 (α5β2γ1) necessary for signal transduction and cell adhesion [22,26,27]. Here, we investigate the role of collagen (IV) isoform homeostasis in a diabetic podocytopathy model established from human iPS cell-derived podocytes.

## Results

### *Establishment and characterization of the diabetic podocyte injury model*

To establish a stem cell-derived model of diabetic podocytopathy, we first differentiated human iPS cells into mature glomerular podocytes using established methods [28–30], and then maintained the cells for up to 4 weeks at normal (5 mM) or high (25 mM) blood glucose levels with and without 1 ng/mL each of the inflammatory cytokines IL-6 and TNFα **(**Fig. 1**A).** By day 9 of treatment with the high-glucose conditions, retraction of podocyte foot processes was observed, and it worsened over time **(**Fig. 1**B,** Supplementary Fig. 1**A).** These morphological changes were accompanied by statistically significant decrease in cell viability **(**Fig. 1**C)** and dysregulated (low or excessive) expression levels of nephrin and lower podocin **(**Fig. 1**D and E,** Supplementary Fig. 1**B)** in the high-glucose cultures compared to the normal-glucose control. Previous studies have shown that both nephrin deficiency and the inflammatory cytokines, IL-6 and TNFα, are activators of NF-κB signaling that normally regulates immune responses and cell survival but plays a role in the pathogenesis of DN and progression to ESKD [31–35]. Podocin is a lineage restricted protein that also forms a complex with other scaffolding proteins at the podocyte foot processes. Between days 16 and 17, we observed significant podocytopenia in the high-glucose conditions **(**Fig. 1**F and G)**, a characteristic podocyte injury response preceding proteinuria *in vivo* and *in vitro* [36]. Thus, the human iPS cell-derived model revealed an association between hyperglycemia and molecular and morphological impairment in podocytes that manifests as loss of foot process integrity and cell detachment from the substrate, both of which have implications for uncovering previously unknown mechanisms of DN and advancing strategies for precision medicine applications.

### *ECM remodeling in diabetic podocyte injury*

The magnitude of cell detachment in the high-glucose podocyte cultures prompted us to investigate changes at the podocyte-ECM interface. We examined the spatial and temporal deposition patterns of collagen (IV)α1, the primary ECM protein deposited by podocytes *in vivo* during development [22–24]. We observed excess deposition of collagen (IV)α1 by the podocytes exposed to high-glucose medium (with and without IL-6 and TNFα) starting at day 9 **(**Fig. 2**A-D)**, which coincided with the onset of podocyte foot process retraction. Although severe podocytopenia in the high-glucose cultures was observed at day 16, cells that remained adhered exhibited lower collagen (IV)α1 expression levels than the normal-glucose control **(**Fig. 2**A,** Supplementary Fig. 2**A)**, which could result from matrix remodeling and ECM loss during podocyte detachment. Furthermore, compared to the control group, we found that diabetic injury resulted in an increase in collagen (IV)α1 deposition that was spread over the field of view, such that more cells were covered with or bound to higher amounts of ECM **(**Fig. 2**B and C).** Linear regression analysis of injury progression data confirmed that a significant difference in collagen (IV)α1 deposition pattern emerged after day 9 of treatment with high glucose conditions **(**Fig. 2**D).**

Western blot and RT-qPCR analysis revealed that podocytes in hyperglycemic conditions build up intracellular gene and protein expression of collagen (IV)α1 by day 5, prior to its increased extracellular deposition and the observed foot process retraction at day 9 **(**Fig. 2**E-G,** Supplementary Fig. 2**B).** However, we found that there was no disruption to Nidogen gene expression, a matrix protein that links laminin and collagen (IV), and lower expression of TWIST-1, a marker of epithelial-to-mesenchymal transition **(**Supplementary Fig. 2**B)**, demonstrating the importance of collagen (IV) dysregulation as one of the earliest responses to injury. While there was a significant increase in collagen (IV)α3 gene expression at day 5 for high glucose podocytes with inflammatory cytokines, there was no difference in collagen (IV)α3 deposition amongst the treatment conditions by day 9. **(**Supplementary Fig. 2**C).** Interestingly, on day 5, both hyperglycemia-injured podocytes accumulated more collagen (IV)α1 than collagen (IV)α3 (the primary ECM protein or collagen isoform produced by mature podocytes). By day 16, little to no collagen (IV)α1 was expressed by the cells that remained adhered, consistent with the microscopy results.

Based on these findings, we hypothesized that the time-dependent remodeling of the podocyte ECM could be associated with changes in the ECM's structure. To examine this possibility, we decellularized the podocyte ECM (after 13 days of treatment with high glucose) and examined the ECM structure by scanning electron microscopy. We observed overall higher levels of ECM deposition in the hyperglycemic conditions than in the normal-glucose control. Intriguingly, thicker ECM fibers were observed in the high glucose with IL-6 and TNFα condition than in high glucose without the inflammatory cytokines **(**Fig. 2**H).** Taken together, these results reveal a dynamic profile of an embryonic isoform of collagen (IV) underlying podocyte response to hyperglycemic conditions.

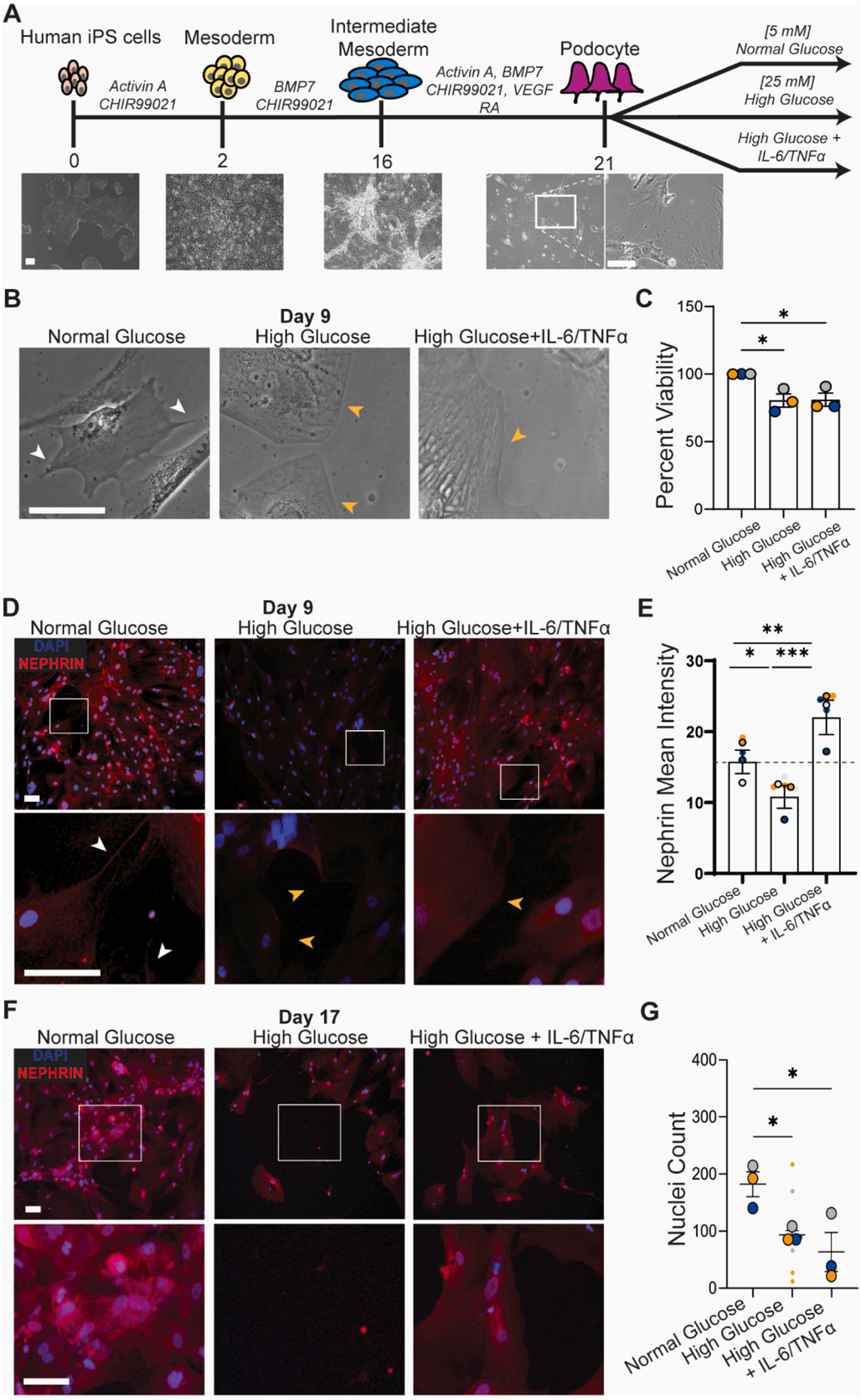


(caption on next page)

**Fig. 1. Establishment and characterization of the diabetic injury model. A.** Schematic and representative brightfield microscopy images of podocyte derivation from human iPS cells (adapted from Musah et al. 2017) and culture conditions for diabetic injury. **B.** Brightfield images highlighting the structure of podocyte foot processes in health and disease. White arrows indicate primary cell processes/extensions in normoglycemia; yellow arrows indicate foot process retraction from diabetic injury. **C.** Podocyte viability at day 9 diabetic injury, n = 3 color-matched biological replicates (WST-8/CCK8 assay) **D.** Immunofluorescent images showing differential nephrin expression in podocyte foot processes from diabetic injury (DAPI, blue; nephrin, red). **E.** Quantification of nephrin mean intensity per field of view. Baseline expression level denoted as dotted line; n = 4 images for normal glucose, n = 6 images for high glucose and high glucose + IL-6/TNFα. **F.** Immunofluorescence images showing severe podocyte detachment upon prolonged exposure to diabetic conditions (DAPI, blue; nephrin, red). **G.** Nuclei (DAPI) count of injured podocytes at day 17 of culture; n = 3 color-matched biological (large dots) and technical (small dots) replicates. **A-C, E** Scale bars, 100 μm. **D,F** Data are mean ± S.E.M. *p < 0.05; **p < 0.01; ***p < 0.001. (For interpretation of the references to color in this figure legend, the reader is referred to the web version of this article.)

*Cell detachment from collagen (IV)α1α1α2-rich matrix is unique to podocytes*

Increased glomerular filtration barrier permeability from hyperglycemia has been attributed to the detachment of podocytes from the GBM. Meanwhile, endothelial cells are well known for their loss of fenestrations and stress signaling (e.g. high reactive oxygen species, inflammatory cytokines, etc.) when exposed to injury[37], but their contribution to GBM dysfunction is less known. We examined whether endothelial cells exposed to hyperglycemic conditions also exhibit excess collagen (IV)α1α1α2 deposition and cell detachment as observed for the hyperglycemia-injured podocytes. We derived isogenic vascular endothelial cells from the same human iPS cell line as used to generate podocytes using a previously established method [20,38,39] **(**Fig. 3**A).** At the end of the differentiation period, we began treatment with normal (5 mM) and high (25 mM) glucose. At day 17 (within the same time point noted for the onset of podocyte detachment), we observed no significant reduction in endothelial cell density in the high-glucose culture condition **(**Fig. 3**B).** On day 26 of culture, there was still no change in overall cell density, but the high-glucose-treated cells showed increased expression of platelet endothelial cell adhesion molecule (PECAM/CD31) **(**Fig. 3**C-E),** a pro-adhesive stress response protein [40]. The deposited ECM from these cells also exhibited increased collagen (IV)α1 content **(**Fig. 3**F),** similar to the ECM of hyperglycemia-injured podocytes. *In vivo*, PECAM mediates the inflammatory response of the vasculature that activates TGF-β/SMAD signaling and glomerulosclerosis[41–44]. Additionally, hyperglycemia altered the deposition pattern of endothelial ECM such that there was a significant increase in collagen (IV)α1 coverage and intensity **(**Fig. 3**G-I).** These results suggest that hyperglycemia can induce injuries to both podocytes and endothelial cells such that they both contribute to GBM thickening, but the two cell types have different phenotypic responses to the altered ECM deposition profile — thus, cell detachment for podocytes and sustained adhesion for vascular endothelial cells. In the mature kidney's glomerular filtration barrier, vascular endothelial cells primarily deposit collagen (IV)α1α1α2 while podocytes deposit both collagen (IV)α1α1α2 and collagen (IV)α3α4α5 [23]. The balance between these collagen (IV) isoforms may be critical to the glomerular filtration barrier integrity, and hyperglycemic injury may contribute to increased permeability through dysregulation of the ECM composition accompanied by podocyte loss.

*Dynamics of ECM remodeling in hyperglycemia is distinct from drug-induced injury*

We wanted to understand how hyperglycemic podocyte injury compared to other acute and chronic diseases resulting from nephrotoxicity, and whether we could further define the role of collagen (IV)α1α1α2 in kidney dysfunction. Therefore, we designed parallel experiments involving multiple injury models to help distinguish between the characteristics of hyperglycemia, Adriamycin, and bisphosphonate (pamidronate). Adriamycin has been used to treat a variety of cancers, but this drug is also associated with severe side effects, including nephrotoxicity and acute kidney failure [45]. Adriamycin is widely used in research laboratories to model focal segmental glomerulosclerosis (FSGS) *in vivo* and *in vitro* [17,20,28,46,47]. FSGS can also be caused by the drug pamidronate [48], which is prescribed to treat hypercalcemia and bone-related diseases. We cultured podocytes under normal and high glucose conditions, or in the presence of clinically relevant doses of Adriamycin (0.5 μg/mL) or pamidronate (100 nM) for up to 9 days **(**Fig. 4**A).** Within 24 h of treatment, there was noticeable foot process retraction and podocytopenia in the Adriamycin-treated cells than in all other treatment conditions or injury models evaluated in this study. At 48 h, increased cellular hypertrophy was observed in the pamidronate-treated podocytes, but there was no difference in cell density compared to the control group **(Supplementary** Fig. 3**A).** When Adriamycin and pamidronate were removed from the culture media at 24 h and 48 h, respectively, the podocyte injury phenotypes described above persisted up to day 9 **(**Fig. 4**B, Supplementary** Fig. 3**B).**

We assayed for cell viability at early (day 1) and extended (day 9) injury time points. There was no significant decline in viability for pamidronate-treated podocytes at either time points. In contrast, Adriamycin treatment induced a 40 % decrease in cell viability by the end of day 1 and an additional 40 % reduction by day 9, despite removal of the drug after 24 hr **(**Fig. 4**C).** Within a day of hyperglycemic injury, we observed a 20 % increase in viability compared to normoglycemic podocytes. We attribute this initial observation to an immediate increase in metabolic processing of the glucose-rich microenvironment as a significant decrease in podocyte viability was detected after 9 days of chronic hyperglycemic exposure **(**Fig. 4**C).**

We also assessed molecular level changes related to collagen (IV)α1α1α2 expression and deposition. By day 9, podocyte injury from Adriamycin treatment caused foot process retraction but not excess deposition of collagen (IV)α1. In contrast, both hyperglycemia- and pamidronate-induced injury caused increased expression and excess deposition of collagen (IV)α1 **(**Fig. 4**D-F, Supplementary** Fig. 3**C).** Commonly, none of the treatment groups excessively deposited collagen (IV)α3 **(Supplementary** Fig. 3**D).**

Next, we explored why hyperglycemia but not pamidronate treatment caused podocyte detachment although both caused increased collagen (IV)α1α1α2 deposition. We initially examined the dynamics of ECM remodeling related to protein production and degradation. Collagen (IV)α1α1α2 is more susceptible to proteolytic degradation by MMPs than collagen (IV)α3α4α5 due to lower interchain disulfide bond density [25]. We found that on day 9 of culture, Adriamycin-injured podocytes secreted three times more active gelatinases (MMP-2 and MMP-9 that cleave collagen (IV)) compared to normal glucose, whereas hyperglycemia- and pamidronate-injured podocytes showed no significant changes (Fig. 4**G**). Interestingly, we observed higher expression levels of tissue inhibitor of metalloproteinase-1 (TIMP-1) in pamidronate-treated podocytes than in hyperglycemia-injured podocytes **(**Fig. 4**H and I).** This result may explain why podocyte detachment was not observed in the pamidronate-treated podocytes.

In Fig. 5, we illustrate the common and distinct modes of injury as they relate to podocyte-ECM interactions and remodeling. Our results suggest that the mechanisms of Adriamycin-induced injury differ from those caused by exposure to pamidronate or hyperglycemic conditions. In contrast, increased expression and deposition of collagen (IV)α1α1α2 is a shared response among pamidronate- and hyperglycemia-injury, but hyperglycemia-injured podocytes are more susceptible to detachment

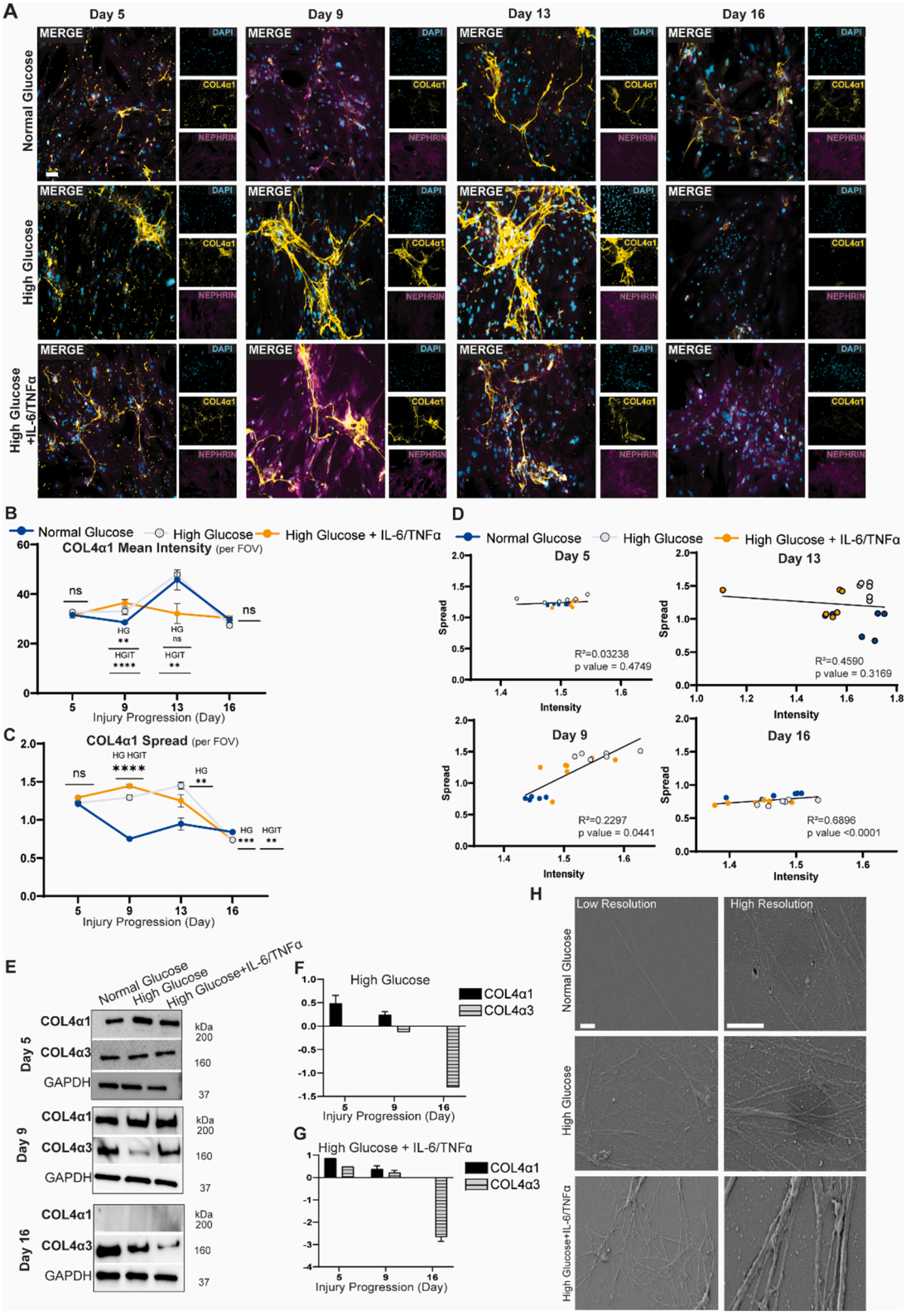


**Fig. 2. Characteristic ECM remodeling correlates with diabetic injury progression. A.** Immunofluorescence images of podocyte (DAPI, cyan; nephrin, magenta) collagen (IV)α1 deposition (COL4α1, yellow) over diabetic injury progression. **B.** Quantification of collagen (IV)α1 mean intensity per field of view; n = 6 images per condition. **C.** Quantification of collagen (IV)α1 spread per field of view; n = 6 images per condition. **D.** Linear regression analysis of spread vs. intensity on days 5, 9, 13, and 16 of diabetic injury **E.** Western blot images of embryonic and mature isoforms of collagen (IV), α1 and α3, respectively, over diabetic injury progression. **F.** Densitometric analysis of collagen (IV) α1 and α3 during hyperglycemic injury progression, relative to GAPDH and fold change of the normal glucose control condition. **G.** Densitometric analysis of collagen (IV) α1 and α3 of hyperglycemic with inflammation injury progression, relative to GAPDH and fold change of the normal glucose control condition. **H.** SEM of decellularized podocyte ECM at high and low resolution. Scale bars, 100 μm (**A**) and 2 μm (**H**). **B-D** *p < 0.05; **p < 0.01; ***p < 0.001; ****p < 0.0001. (For interpretation of the references to color in this figure legend, the reader is referred to the web version of this article.)

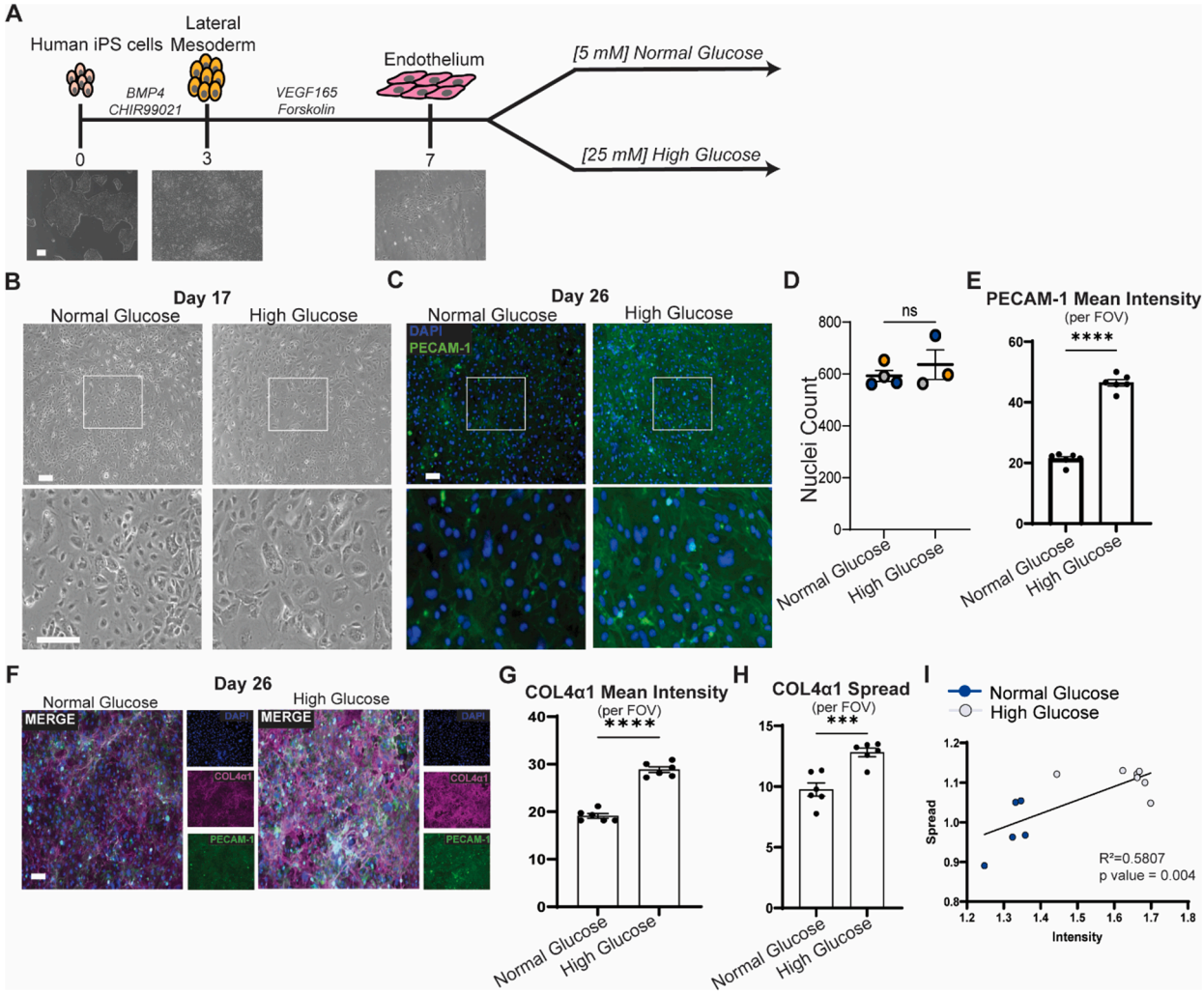


**Fig. 3. Excess collagen (IV)α1α1α2 deposition common among glomerular cell types; cytopenia specific to podocytes. A.** Schematic and brightfield microscopy images of vascular endothelium derivation from human iPS cells (adapted from Atchinson et al. 2017) and culture conditions for diabetic injury. **B.** Brightfield microscopy images of healthy and injured vascular endothelial cell phenotype, time-matched to podocytopenia (day 17). **C.** Immunofluorescence images of PECAM-1 expression (green) in healthy and injured vascular endothelium (DAPI, blue) after 26 days of injury. **D.** Nuclei (DAPI) count of injured endothelial cells at 26 days of culture; n = 3 color-matched biological replicates. **E.** Quantification of PECAM-1 mean intensity per field of view; n = 6 images per condition. **F.** Immunofluorescence images of endothelial cell (DAPI, blue; PECAM, green) collagen (IV)α1 deposition (COL4A1, magenta) at 26 days of injury. **G.** Quantification of collagen (IV)α1 mean intensity per field of view; n = 6 images per condition. **H.** Quantification of collagen (IV)α1 spread per field of view; n = 6 images per condition. **I.** Linear regression analysis of collagen (IV)α1 spread vs. intensity at 26 days of endothelial cell exposure to normal and high glucose conditions; n = 5 images for normal glucose, n = 6 images for high glucose. **A-C, F** Scale bars, 100 μm. **D, F-H** *p < 0.05; **p < 0.01; ***p < 0.001; ****p < 0.0001. (For interpretation of the references to color in this figure legend, the reader is referred to the web version of this article.)

because of a lower inhibition of ECM degradation (associated with lower TIMP-1 expression). Our results suggest that collagen (IV)α1α1α2 ECM remodeling can significantly contribute to kidney disease progression.

### *Signals from healthy ECM can attenuate hyperglycemic podocyte injury phenotype*

Because human kidney podocytes have no known regenerative capacity and are implicated in the most devastating forms of DN and ESKD, there is a growing interest to develop targeted regenerative medicine strategies for podocytopathies. We hypothesized that changes in ECM composition and remodeling, such as those described in this study, could be targeted to ameliorate the effects of hyperglycemia-induced podocyte injury. To examine this possibility, we isolated ECM scaffolds from podocytes grown for 9 days in normal glucose (NG) and high glucose (HG) and determined whether the healthy ECM scaffold could encourage the repair of hyperglycemia-injured podocytes (Fig. 6**A).** We used immunofluorescent microscopy and RNA isolation to confirm that the decellularized scaffolds retained collagen (IV) expression that was free of genetic material (both DNA and RNA) (Fig. 6**B and C**, **Supplementary** Fig. 4**A).** Podocytes cultured for 9 days in normal glucose and high glucose conditions were repopulated onto the NG and HG scaffolds and cultured for an additional 2 days in their respective media. We observed that normal glucose and high glucose podocytes on their respective NG and HG scaffolds retained their characteristic morphologies: primary and secondary foot processes in healthy cells, foot process retraction in injured cells **(**Fig. 6**D).** To investigate molecular level changes related to ECM adhesion, we probed two mechanosensitive proteins essential for podocyte health and homeostasis: yes-associated protein (YAP) and synaptopodin, as well as an important foot process protein, podocin. Nuclear localization of YAP is essential for podocyte function and survival. We have previously shown that gene expression of YAP is unaffected by Adriamycin-induced podocytopathy but upregulated in hyperglycemia-injured podocytes [17]. In this study, we found that YAP was significantly translocated from the nucleus to the cytoplasm after 9 days of hyperglycemic injury (Fig. 6**E**). We also observed

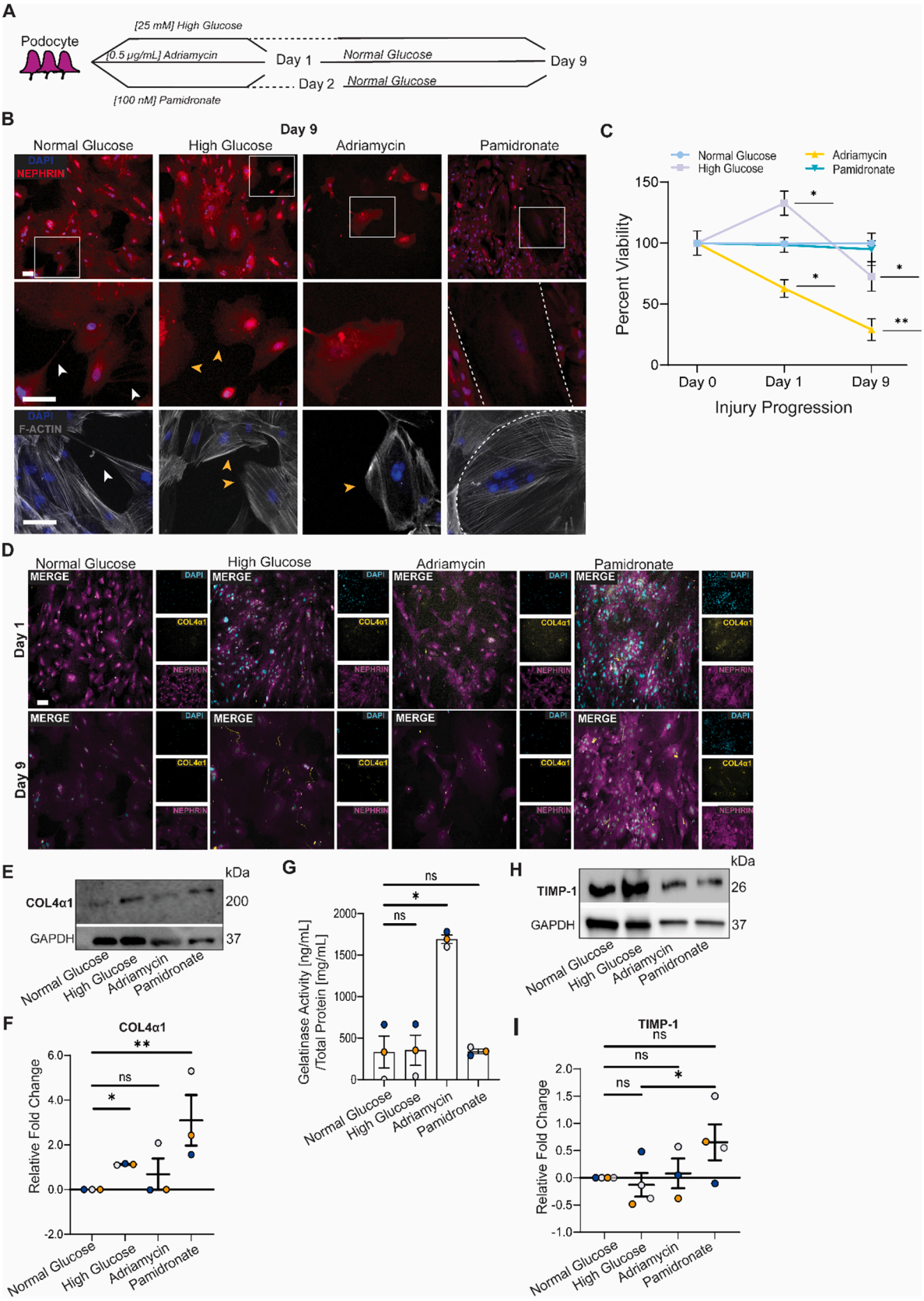


(caption on next page)

**Fig. 4. ECM remodeling mechanism in hyperglycemia is distinct from drug-induced injury A.** Schematic of the experimental strategy for hyperglycemia- and drug-induced disease treatments. **B.** Immunofluorescence microscopy images of podocyte foot process morphology (top and middle row panels: DAPI, blue; nephrin, red) and actin cytoskeleton (bottom row panel: DAPI, blue; F-actin, gray) via hyperglycemia- and drug-induced injury. White arrowheads indicate primary and secondary foot processes, yellow arrowheads indicate foot process retraction, dashed lines denote cell body perimeter **C.** Podocyte viability before and after hyperglycemia- and drug-induced podocyte injury; n = 3. **D.** Immunofluorescence images of podocytes (DAPI, cyan; Nephrin, magenta) collagen (IV)α1 (magenta) deposition in hyperglycemia- and drug-induced injury. **E.** Western blot analysis of embryonic isoform collagen (IV)α1 following nine days of injury. **F.** Densitometric analysis of collagen (IV)α1 after nine days of injury.; n = 3. **G.** Gelatinase (MMP-2 and MMP-9) activity normalized to total protein; n = 3 color matched biological replicates. **H.** Western blot of TIMP-1 expression after 9 days of injury. **I.** Densitometric analysis of TIMP-1 levels after 9 days of injury; n = 3 color-matched biological replicates for Adriamycin, n = 4 color-matched biological replicates for all other conditions. **B, D** Scale bars, 100 μm. **C, F, G, I** *p < 0.05; **p < 0.01. (For interpretation of the references to color in this figure legend, the reader is referred to the web version of this article.)

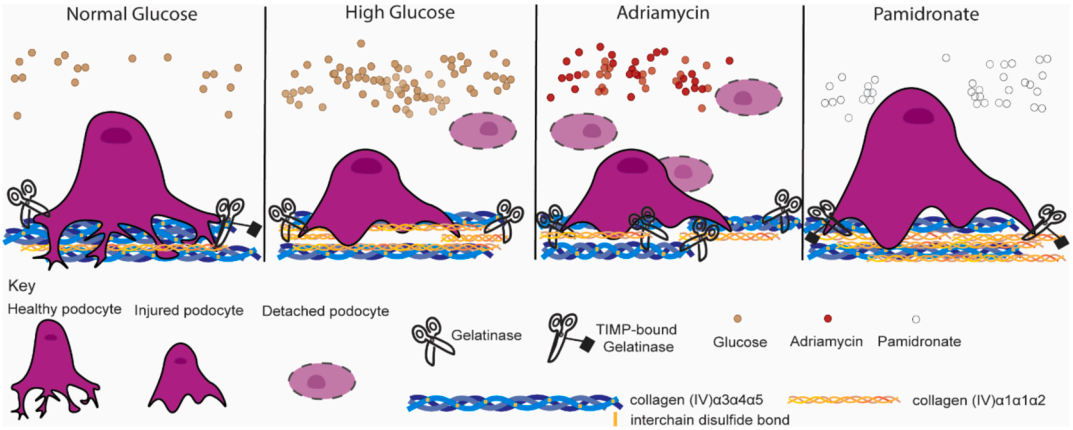


**Fig. 5. Proposed model for podocyte-ECM interactions and matrix remodeling in distinct injury modes.** Higher collagen (IV)α1α1α2 deposition, mediated by a hyperglycemic microenvironment, results in podocyte detachment despite similar levels of gelatinase activity compared to normoglycemia due to differences in interchain disulfide bond density. Podocyte exposure to Adriamycin results in no significant changes to ECM composition but cell detachment is mediated by dramatically higher gelatinase activity. Pamidronate exposure causes higher collagen (IV)α1α1α2 deposition but does not result in immediate podocyte loss or detachment, partly due to elevated gelatinase inhibition by TIMP-1.

varying patterns of YAP migration, depending on the cell state and scaffold composition: when normal glucose podocytes were transferred to HG scaffolds, nuclear YAP increased, whereas on NG scaffolds, cytoplasmic YAP increased. Despite similar levels of nuclear YAP, increased cytoplasmic YAP in the healthy podocytes may relate to actin rearrangements on the new matrix to which the cells were transferred. When high glucose podocytes were transferred to HG scaffolds, cytoplasmic YAP decreased, whereas on NG scaffolds, nuclear YAP was partially restored (Fig. 6**E,** Supplementary Fig. 4**B-D**). These results indicate that the cells can transduce extracellular signals from the scaffolds into intracellular molecular changes. Next, we assessed the podocyte structure via podocin. We observed that the healthy podocytes sequestered podocin at the cell edge, a phenotype that was lost due to high glucose exposure (Fig. 6**F**). On the HG scaffolds, we found a mixed phenotype of podocin at the cell edge and some remained in the cell body. However, on the NG scaffolds, we found that podocytes exposed to both normal and high-glucose conditions have podocin sequestration at the cell edges, despite the high-glucose cells still being in the hyperglycemic microenvironment. In addition to the podocin observations, were also confirmed that nephrin and vinculin are intracellularly expressed in all conditions via western blot, both of which are important proteins for cell–cell and cell-matrix integrity, respectively (Supplementary Fig. 4**B**). Of note, western blot analysis showed that nephrin expression was generally decreased in the scaffold groups, whereas the immunostaining results closely aligned with the observed podocin expression profile. Additionally, foot process retraction was more pronounced in the normal glucose podocytes propagated on HG scaffolds, whereas elongation at the cell edge was more evident in the high glucose cells on NG scaffolds compared to their respective native ECM control (Supplementary Fig. 4**E**). Finally, we probed synaptopodin, an actin-associated protein that regulates stress fiber formation in motile and contractile cells. Synaptopodin (108 kDa) expression was reduced in hyperglycemia-injured podocytes, yet this loss was attenuated in hyperglycemia-injured podocytes only when the cells were propagated on the NG scaffold, and not on the HG scaffold (Fig. 6**G-I,** Supplementary Fig. 4**F and G**). These results underscore synaptopodin plasticity in human kidney glomerular podocytes. The results on YAP, podocin, nephrin, and synaptopodin expression also suggest that signals from healthy ECM could be explored in the future to potentially halt or repair hyperglycemia-induced podocyte injury. We anticipate that these findings could open new avenues for targeting podocytopathies and DN.

## Discussion

Diabetes mellitus is a systemic metabolic disease characterized by altered glucose homeostasis. A significant number of diabetic patients are at risk of severe complications including neuropathy, heart disease, or chronic wounds [49]. Physiological tissue barriers are affected by diabetes including the glomerular filtration barrier (diabetic nephropathy, the focus of this study), blood–brain barrier (diabetic neuropathy), blood-retinal barrier (diabetic retinopathy), skin barrier (chronic diabetic wounds) [50], and intestinal barrier (leaky gut syndrome) [51]. While treatments exist for some of these injuries and help partially restore the structural and functional integrity of the impaired barriers, no targeted therapy exists to repair or regenerate kidney tissues compromised by DN.

Renal regenerative medicine aims to advance the use of stem cells for pathophysiological modeling and tissue replacement. The desire to achieve this objective encourages the generation of patient-specific and immunocompatible solutions to disease. This study demonstrates the flexibility of human iPS cells to derive multiple cell types relevant to the kidney (podocytes and vascular endothelial cells) and to recapitulate multiple models of nephrotoxicity in parallel to identify distinct responses (chronic hyperglycemia- and drug-induced podocytopathies).

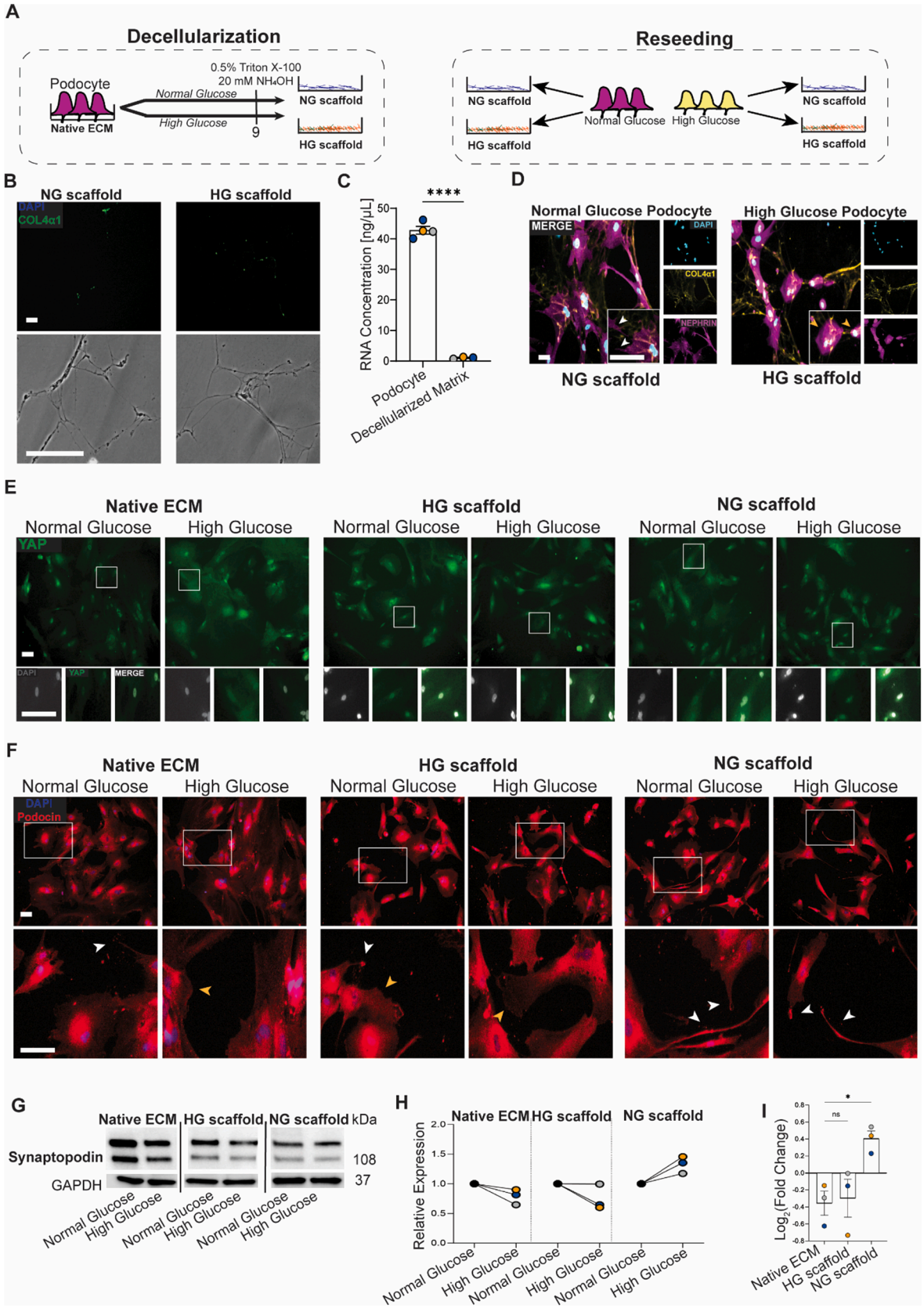


(caption on next page)

**Fig. 6. Signals from healthy matrix can attenuate hyperglycemic injury phenotype. A.** Schematic of experimental strategy to isolate and repopulate normal glucose (NG) and high glucose (HG) podocyte-derived ECM scaffolds. **B.** Analysis of ECM scaffold genetic material via immunofluorescence microscopy of nuclei (top panel; DAPI, blue) and brightfield microscopy. **C.** ECM scaffold mRNA quantification; n ≥ 3 color-matched biological replicates. **D.** Immunofluorescence images of normal glucose and high glucose podocytes (DAPI, cyan; nephrin, magenta) adherence to their respective ECM scaffolds (COL4α1, yellow). White arrowheads indicate primary and secondary foot processes, yellow arrowheads indicate effacement. **E.** Immunofluorescence images of YAP (green) localization in healthy and injured podocytes (DAPI, greyscale) on ECM scaffolds. **F.** Immunofluorescence images of podocyte morphology (DAPI, blue; podocin, **red)** on decellularized scaffolds **G.** Western blot of synaptopodin expression (bottom band) of healthy and injured cells on ECM scaffolds. **H.** Densitometric analysis of synaptopodin expression relative to GAPDH; n = 3 color matched biological replicates. **I.** Fold change of synaptopodin expression compared to normal glucose control on the same substrate. **B, D-F** Scale bar, 275 μm; inset scale bar, 90 μm. **C and I***$p < 0.05$; **$p < 0.01$; ***$p < 0.001$; ****$p < 0.0001$. (For interpretation of the references to color in this figure legend, the reader is referred to the web version of this article.)

As a proof-of-concept, we demonstrated that human iPS cell-derived model of podocyte injury can help investigate diabetic glomerulosclerosis, ECM remodeling, and cell-matrix interactions. Lineage-restricted marker expression (e.g. nephrin, podocin, synaptopodin, etc.) is a dynamic process that is spatiotemporally controlled and adjusts according to the cell's needs but can become severely dysregulated in response to injury. It has been reported that diabetic kidney disease (normo- to macroalbuminuria) results in both downregulation of nephrin expression in human and animal glomerular biopsies [52–54] as well as elevated nephrin secretion, or nephrinuria, in clinical trials [55–57], both of which contribute to the progression of proteinuria. The use of human iPS cell-derived podocytes as pursued in this study can illuminate the variable expression levels of nephrin and other critical proteins when exposed to the hyperglycemic microenvironment. Notably, these disease models can be probed even at early stages of injury than can be achieved using traditional approaches (including Streptozotocin or high fat diet) animal models and patient studies where proteinuria and sometimes severe tissue damage has already occured – an essential step towards the identification of biomarkers for early detection of disease. Additionally, we found that collagen (IV)α1α1α2 was intracellularly expressed and extracellularly deposited for a majority of the study's timeframe but eventually reduces, in congruence with gene level analyses in other developmental models and clinical samples [23,24,58,59]. The protein's function in adult podocyte homeostasis and its association with collagen (IV) α1α2α1(IV) produced by the endothelium or mesangial cells is an open research question. It also remains undetermined what molecular signaling pathways are triggered by and mediates this collagen isoform switch from health to diabetic injury. We showed that the dynamics of ECM remodeling by podocytes can differ depending on injury stimuli despite shared observed clinical phenotypes (e.g., glomerular basement membrane thickening, proteinuria, etc.). Such molecular level differences and cellular responses could guide the development of targeted treatments.

We explored the feasibility of our model to respond to bioengineered therapies using ECM scaffolds that were decellularized from human iPS cell-derived podocytes. It was found that some of the diseased podocyte characterizations improve if the cells are provided or interfaced with a healthy ECM, especially synaptopodin, which has been shown to be protective against acute podocyte injury [60]. This work could inform the design of more robust, mechanically stimulating ECM-based systems or strategies to engage the podocyte contractile apparatus and potentially repair the slit diaphragm and reverse tissue damage.

Previous studies of human renal biopsy and animal kidney models have revealed lesions of collagen (IV)α1α1α2 in advanced stage diabetic nephropathy [61,62]. Similarly, Iglesias de la Cruz *et al.* demonstrated that chronic (2-weeks) high glucose or TGF-β exposure (for 24 hr) increased collagen (IV) α1 and α5 mRNA and protein expression in immortalized mouse podocytes[63]. Our model advances this set of knowledge by demonstrating spatiotemporal dynamics of collagen (IV)α1α1α2 specifically in human podocytes during disease onset and progression, such that excess deposition of this embryonic isoform of collagen (IV) coincides with podocyte retraction of their foot processes and subsequent podocytopenia. Our SEM results are consistent with previous findings from injured human and mice glomerular tissues in that denuded or decellularized glomerular basement membranes have increased ECM fiber density but exhibit a more patchy and uneven appearance [64,65]. In support of our strategy, the GBM is being targeted for tissue repair by modulating cellular responses or manipulating ECM composition [21,64,66]. For example, LeBlue and colleagues (2024) recently explored human stem cell-based therapeutic strategies for Alport syndrome by engineering a novel allele to show that podocytes (not endothelium) are the predominant facilitators of collagen (IV) α3 chain production and that collagen (IV) α3-deficient kidneys can improve in function if provided the protein via horizontal gene transfer from allogenic bone marrow-derived mesenchymal cells or iPS cells [67].

Future work could explore whether our results translate to complex human-relevant systems, including organ-chip devices or human stem-cell derived organoids [18,20,68]. Additionally, while we found that signals in healthy matrix derived from podocytes can attenuate the hyperglycemic injury phenotype, future work might explore whether the transferred podocytes retain a mechanical memory (or epigenetic remodeling), which would have implications for the use of iPS cell-based therapies in regenerative medicine [69,70]. Future work could also aim to enhance the translatability of the healthy podocyte-derived ECM scaffold, which is limited *in vivo* due to ethical concerns and the challenge of repopulating scaffolds within the kidney's complex tissue architecture. At the cellular and tissue levels, this work can inform future studies related to repopulation of decellularized organs and scaffolds, a rapidly evolving field within tissue engineering that intends to address the shortage of transplantable organs [71,72].

In conclusion, we established a human stem cell-derived model that recapitulated hallmarks of DN affecting glomerular podocytes. The model revealed a podocyte response to diabetic injury that is not shared with vascular endothelial cells or with chronic or acute drug-induced injury – increased expression and excess deposition of collagen (IV)α1α1α2 that precedes cell detachment. We found that healthy ECM can improve molecular level changes associated with hyperglycemic podocyte injury. Together, these results may inform future strategies to develop targeted therapies that can potentially halt and repair damaged podocytes, a cell type that is not directly protected by anti-hyperglycemic drugs currently available to affected patients.

## Experimental procedures

### *Human iPS cell culture*

The PGP-1 human iPS cell line was obtained from the Personal Genome Project under approved material transfer agreements, and its use was approved by the institutional review board and the stem cell research oversight committee at Duke University. The DU-11 (Duke University clone #11) iPS cell line was generated at the Duke iPSC Core Facility and provided to the Musah Lab by the Bursac Lab at Duke University. The cells were tested and found to be karyotypically normal and free of mycoplasma contamination (Mycoplasma PCR Detection Kit; amb, G238) before use. Human iPS cells were cultured under feeder-free conditions in tissue culture treated 6-well plates (Corning, 353046) coated with hESC-grade Matrigel (Corning, 354277) by following established methods [28,73]. Cells were fed daily with mTeSR1 (Stem Cell Technologies, 85850) and incubated at 37 °C and 5 % $CO_2$. At 70 %

confluence, the cells were dissociated with Accutase (Life Technologies, A1110501) and passaged into a new Matrigel-coated 6-well plate at a 1:6 splitting ratio.

*Derivation of mature podocytes from human iPS cells*

PGP-1 iPS cells at 70 % confluence were incubated with enzyme-free cell dissociation buffer (Gibco, 13150–016) and pelleted via centrifugation at 200 *xg* for 5 min. Podocytes were derived from human iPS cells according to previously established methods [28–30]. Briefly, the human iPS cells were resuspended in mesoderm induction medium and seeded at 100,000 cells/well onto a 12-well plate coated with laminin-511 E8 (Takara Bio, T304). After 2 days of culture, mesoderm cells were differentiated into intermediate mesoderm (IM) cells in IM induction medium for 14 days. To induce podocyte differentiation, IM cells were first dissociated by incubation with 0.05 % trypsin-EDTA (Gibco, 25300054), pelleted via centrifugation, resuspended in podocyte induction medium, and seeded at 150,000 cells/well with daily medium replenishment for up to 5 days.

*Derivation of vascular endothelial cells from human iPS cells*

Vascular endothelial cells were derived according to previously established methods and optimized for cell lines [20,38,39].. Briefly, human iPS cells were dissociated and pelleted, and then resuspended in mTeSR1 medium and seeded at 45,000 cells/cm$^2$ onto Matrigel-coated 6-well plates. The next day, the medium was changed to N2B27 medium to induce lateral mesoderm cells and cultured without changing the medium for 3 days. On day 4, N2B27 medium was replaced with endothelial induction medium that was replenished every day for 3 days. On day 7, vascular endothelial cells were isolated via magnet-activated cell sorting (MACS, Militenyi Biotec). Briefly, cells were prepared incubated with Accutase, and the cell suspension diluted 1:1 with StemPro-34 (Gibco, 10639011) and pelleted via centrifugation. The cell pellet was washed with MACS buffer (Dulbecco's phosphate buffered saline (DPBS, Gibco 14190144), 0.5 % bovine serum albumin (BSA, Millipore Sigma A9418), 2 mM Ethylenediaminetetraacetic acid (EDTA, Thermo Scientific R1021)), and resuspended in 80 μL/10 million cells MACS buffer and 20 μL/10 million cells each of FcR blocking reagent (Militenyi Biotec, 130–059-901), CD31 Microbeads (Militenyi Biotec, 130–091-935), and CD144 Microbeads (Militenyi Biotec,130–097-857). Following 15 min incubation, cells were washed with MACS buffer and sorted on a QuadroMACS Separator (Militenyi Biotec, 130–091-051). CD31+/CD144 + cells were expanded in conditioned medium diluted at a 1:1 ratio with StemPro-34 supplemented with 2 μg/mL heparin (StemCell Technologies, 07980) that was replaced every other day. At 90 % confluence, the cells were passaged up to 1:4 split or used for downstream experiments.

*Propagation of differentiated cells and induction of disease phenotypes*

Healthy podocytes and vascular endothelial cells were maintained at normal blood glucose level (5 mM) in Culture Boost-R (Cell Systems, 4 N0-500-R) that was refreshed every other day.

To induce hyperglycemic injury, podocytes and vascular endothelium were maintained in Culture Boost-R supplemented with D-Glucose (Sigma, G8769) to obtain 25 mM glucose level for up to 4 weeks or until a significant injury phenotype was observed. To recapitulate hyperglycemia with inflammation, podocytes were maintained in 25 mM glucose medium supplemented with 1 ng/mL each of TNF-α (Gibco, PHC3015) and IL-6 (PeproTech, 200–06) [7] for up to 4 weeks or until injury phenotype was observed. Control cells were cultured in normal (5 mM) glucose conditions. For all cell culture conditions, media were refreshed every other day.

Adriamycin (LC Laboratories, D-4000) and pamidronate (Millipore, 506600) were used to recapitulate drug-induced podocytopathy. Podocytes were maintained in Culture Boost-R supplemented with clinically relevant doses of 0.5 μg/mL Adriamycin for 24 h or 100 nM pamidronate for 48 h to induce injury phenotypes. The drug-treated podocytes were then propagated in Culture Boost-R medium for up to 9 days, and the medium was refreshed every other day.

*Cell viability assay*

Cell Counting Kit 8 (WST-8/CCK8) was used to assay cell viability according to vendor protocol (Abcam, ab228554). Briefly, a master mix of WST-8 solution was made at a 1:10 dilution in the respective solutions for healthy and injured podocytes. The cells were incubated with the solution for 2 hrs at 37 °C, protected from light. The absorbance was measured at 460 nm using an Infinite M200 Pro plate reader (TECAN Group) with Magellan (software version 7.2), and the readouts were normalized to podocytes in normal glucose.

*Gelatinase activity assay*

Gelatinase activity in the cell culture supernatant was assayed using the Innozyme Gelatinase Activity Assay kit (CBA003, Sigma Aldrich) according to the vendor's protocol. The kit, used as provided, is highly selective for MMP-2 and MMP-9 (but does not distinguish the two enzymes). Briefly, cells were cultured for up to 9 days at which time, supernatant was collected and centrifuged at 2,000*xg* for 10 min, pelleted cell debris was discarded. Activation buffer was used to prepare a 2x serial dilution for the provided standards and 1:4 dilution of cell culture supernatant. 90 μL of standard and sample were added to each well of a 96-well plate, in duplicate, and incubated at 37 °C for 6 hrs. Fluorescence was read at 320 nm excitation and 405 nm emission on an Infinite M200 Pro plate reader (TECAN Group) with Magellan (software version 7.2). All values were normalized to total protein.

*Extracellular matrix decellularization*

Cells were gently rinsed twice with 2 mL DPBS (without $Ca^{2+}$ and $Mg^{2+}$). Sterile-filtered, warm extraction buffer (consisting of 0.5 % Triton X-100 (VWR, 97063–996) and 20 mM $NH_4OH$ (Sigma, 221228) in DPBS supplemented with 1 % Penicillin-streptomycin) was added at 500 μL/well to each well of a 12-well plate. The plate was incubated at 37 °C until no intact cells were visible under the microscope (~1–3 min). Without aspirating, the cellular debris was diluted with 1 mL of DPBS (without $Ca^{2+}$ and $Mg^{2+}$) which was added by gentle contact with the sidewall of the plate's well to avoid detachment of the adherent matrix. To remove the extraction buffer, 1–2 mL of the solution was pipetted out from the well such that there was only a thin liquid layer left in each well. 2 mL DPBS (without $Ca^{2+}$ and $Mg^{2+}$) was then added to each well, and the plate was wrapped with parafilm and stored overnight at 4 °C.

*Transfer of live podocytes to decellularized extracellular matrix Scaffolds*

9-day normal and high glucose decellularized ECM scaffolds and live, 9-day normal and high glucose podocyte cultures were prepared as described above. ECM scaffolds were washed twice with 1 mL DPBS (per well) and once with Advanced DMEM/F12. The Advanced DMEM/F12 was then removed by pipette such that there was only a thin layer of fluid to avoid ECM dehydration. Podocyte cultures were then washed once with warm Advanced DMEM/F12, trypsinzed at 37 °C, collected in separate conical tubes with care not to cross-contaminate between conditions, and pelleted via centrifuged. Cell pellets were resuspended in 1 mL of respective Culture Boost medium per new transfer well.

Podocytes were gently seeded onto the ECM scaffolds via the wall of the well to avoid disturbing the matrix, and the plates were moved in figure-eight fashion to evenly distribute the cell suspension. The newly seeded plates were incubated overnight at 37 °C. The respective cell culture media were replenished the next day and every other day from

then on.

*Microscopy analyses*

Cells were prepared at room temperature for immunostaining by fixation in 4 % formaldehyde (Thermo Scientific, 28908) for 20 min, followed by permeabilizing with 0.125 % Triton X-100 in DPBS for 5 min, and blocking with 1 % BSA (Millipore Sigma, A9418-100 g) in 0.125 % Triton X-100/PBS for 30 min. The cells were then washed three times (5 min each) with 0.125 % Triton X-100/PBS. The following primary antibodies were diluted 1:400 in 0.125 % Triton X-100: anti-nephrin (ARP, GP-N2), anti-PECAM-1 (R&D Systems, AF-806), anti-YAP (Santa Cruz Biotechnology, sc-101199), anti-collagen IVα3 (Santa Cruz Biotechnology, sc-52317) and anti-collagen IVα1 (eBioscience, 14–9871-82). The cells were incubated in primary antibody overnight at 4 °C. Following overnight incubation, cells were washed three times for 5 min with 0.125 % Triton X-100/DPBS. The following secondary antibodies were diluted 1:1000 in 0.125 % Triton X-100/DPBS: donkey anti-rabbit Alexa Fluor 594 (Invitrogen, A-21207), donkey anti-mouse Alexa Fluor 488 (Invitrogen, A-21202), and goat anti-guinea pig 594 (Invitrogen, A-11076). DAPI (Invitrogen, D1306; 1:1000 dilution in $H_2O$) or Alexa Fluor 594 Phalloidin (Invitrogen, A12381; 1:1000 dilution in DPBS) were applied to the cells and incubated for 5 min and 15 min, respectively. Brightfield and immunofluorescence microscopy images were acquired with an EVOS M7000 imaging system (Invitrogen, AMF7000) and processed using Fiji/ImageJ (software version 2.9.0/1.54d).

*Scanning electron microscopy*

Podocyte extracellular matrices were decellularized as previously described. Matrices were then fixed with 2.5 % glutaraldehyde in 0.1 M sodium cacodylate buffer (Electron Microscopy Sciences, 11650) for 1 h at room temperature with the plate wrapped in parafilm to avoid evaporation. Each well (containing decellularized ECM) was washed three times (for 10–15 min each) with 0.1 M sodium cacodylate buffer. The matrices were then treated with 1 % osmium tetroxide (Electron Microscopy Sciences, 19180) in 0.1 M sodium cacodylate for 1 h at room temperature with the plate wrapped in parafilm. After washing three times (for 5 min each) with deionized water, the matrices were dehydrated in ascending grades of ethanol: 30 % EtOH for 5 min, 50 % for 5 min, 70 % for 5 min, 80 % for 5 min, 90 % for 10 min, 95 % for 10 min, and 100 % for 10 min. The matrices were then immersed in hexamethyldisilazane (Electron Microscopy Sciences, 16700), which was allowed to evaporate overnight. Samples were coated with gold film using a Denton Desk V (Denton Vacuum), followed by imaging using an Apreo S scanning electron microscope (Thermo Fisher) at the Duke Shared Materials Instrumentation Facility.

*Western blot*

To prepare whole cell lysates, podocytes in 12-well plates were placed on ice and washed twice with ice-cold DPBS. The cells were lysed with ice-cold RIPA buffer supplemented with 1X PhosSTOP phosphatase inhibitor (Millipore Sigma, 04906837001) and protease inhibitor cocktail (Millipore Sigma, 4693132001) per manufacturer recommendations. Protein lysates were quantified using a Pierce BCA protein assay kit (Thermo Fisher, 23227). Protein lysates (5–15 μg) were diluted 3:1 in Laemmli buffer containing 2-mercaptoethanol (Sigma, M3148) and then denatured by incubation at 95 °C for 5 min. The samples were processed using SDS-PAGE with a Mini-PROTEAN TGX Stain-Free Precast 4–15 % gel (Bio-Rad, 4568033). Gels were transferred onto a Midi PVDF membrane using a Trans-blot Turbo semi-dry transfer system. Transferred blots were blocked with 5 % nonfat milk in Tris-buffered saline with Tween-20 (TBS-T) at room temperature for 1 h. For immunoblotting, the following primary antibodies and dilutions were used in 5 % Blotto/TBS-T: anti-COL4A1 (Cell Signaling Technology, 50273; 1:1000), anti-COL4A3 (Santa Cruz Biotechnology, sc-52317; 1:100), anti-synaptopodin (Santa Cruz Biotechnology, sc-515842; 1:500), anti-TIMP-1 (Cell Signaling Technology, 8946; 1:1000), anti-NPHS2 (Abcam, ab50339), anti-vinculin (Invitrogen, PA5-29688), and anti-GAPDH (EMD Millipore, ABS16; 1:4000). Blots were incubated in primary antibody solution overnight on a platform angle rocker at 4 °C. Following overnight incubation, blots were washed three times for 7 min in TBS-T and then incubated for 1 h with secondary antibody HRP-conjugated anti-mouse (Cell Signaling Technology, 7074P2) or anti-rabbit (Cell Signaling Technology, 7074) diluted 1:1000 in 5 % Blotto/TBS-T with rocking at room temperature. The blots were then washed three times with TBS-T for 7 min, followed by band development using the Super Signal West Femto kit (Thermo Scientific, 34094) for 1–5 min. Chemiluminescent bands were imaged using a GelDoc system (Bio-Rad).

*Statistical analysis*

All quantitative results are presented as mean ± standard error of the mean. All statistical analyses were performed with GraphPad Prism version 9.5.1. To compare two unpaired groups with a single variable, the Student's *t*-test with a 95 % confidence interval was used. For comparisons with more than one variable and/or three or more groups of data, an analysis of variance (ANOVA) was performed with an appropriate post-hoc test.

## Data sharing

The datasets generated and analyzed during the study are available from the corresponding author upon reasonable request.

## Sources of funding

This work was funded by a Whitehead Scholarship in Biomedical Research, Chair's Research Award from the Department of Medicine at Duke University, MEDx Pilot Grant on Biomechanics in Injury, Burroughs Wellcome Fund PDEP Career Transition Ad Hoc Award, Duke Incubation Fund from the Duke Innovation and & Entrepreneurship Initiative, Genentech Research Award, George M. O'Brien Kidney Center Pilot Grant (P30 DK081943), and NIH Director's New Innovator Grant (DP2DK139544) awarded to S.M. Y.R. was partially supported by a William M. "Monty" Reichert Graduate Fellowship from the Department of Biomedical Engineering at Duke University and a North Carolina KUH TRIO Fellowship (U2CDK133491, TL1139567). This work was performed in part at the Duke University Shared Materials Instrumentation Facility, a member of the North Carolina Research Triangle Nanotechnology Network that is supported by the National Science Foundation (ECCS-2025064).

## CRediT authorship contribution statement

**Yasmin Roye:** Writing – original draft, Visualization, Methodology, Investigation, Formal analysis, Data curation, Conceptualization. **Carmen Miller:** Data curation. **Titilola D. Kalejaiye:** Methodology. **Samira Musah:** Writing – review & editing, Writing – original draft, Supervision, Resources, Project administration, Methodology, Investigation, Funding acquisition, Conceptualization.

## Declaration of competing interest

The authors declare the following financial interests/personal relationships which may be considered as potential competing interests: S. M. is an inventor on a patent regarding podocyte differentiation, U.S. Patent No. 11,083,754 B2. U.S. Patent and Trademark Office. All other authors declare no other competing interests.

## Acknowledgements

The authors thank Xingrui Mou for assistance with SEM, Miguel Flores-Garcia (AMGEN Summer Research Scholar at Duke University, from UC Berkeley) for technical assistance, and Makenzie Bonner for preliminary experiments on pamidronate-induced podocyte injury, and all members of the Musah Lab at Duke University for comments on the manuscript. The authors also thank Dr. Rasheed Gbadegesin for helpful discussions on the genetic basis of podocyte defects and ECM remodeling, Dr. Morgan Burt (former Musah Lab member) for establishing the YAP colocalization assay used in this study, the Duke Shared Materials Instrumentation Facility as well as students and staff of the Engineering Design POD for assistance with SEM sample preparation; Marcie Pachino from the Graduate Communications and Intercultural Program at Duke University's Pratt School of Engineering, Loren Baugh, and Caroline Conner for manuscript revisions and comments. Y.R. is thankful for the Duke University-Alfred P. Sloan Foundation Scholarship.

## Appendix A. Supplementary data

Supplementary data to this article can be found online at https://doi.org/10.1016/j.mbplus.2024.100164.

## Data availability

Data will be made available on request.

## References

[1] Centers for Disease Control and Prevention. *Chronic Kidney Disease in the United States, 2023*. Atlanta, GA: US Department of Health and Human Services, Centers for Disease Control and Prevention; 2023.
[2] P. Rossing, M.L. Caramori, J.C.N. Chan, H.J.L. Heerspink, C. Hurst, K. Khunti, A. Liew, E.D. Michos, S.D. Navaneethan, W.A. Olowu, T. Sadusky, N. Tandon, K.R. Tuttle, C. Wanner, K.G. Wilkens, S. Zoungas, J.C. Craig, D.J. Tunnicliffe, M.A. Tonelli, M. Cheung, A. Earley, I.H. De Boer, Executive summary of the KDIGO 2022 Clinical Practice Guideline for Diabetes Management in Chronic Kidney Disease: an update based on rapidly emerging new evidence, Kidney Int. 102 (2022) 990–999. https://doi.org/10.1016/j.kint.2022.06.013.
[3] K.P. McCullough, H. Morgenstern, R. Saran, W.H. Herman, B.M. Robinson, Projecting ESRD incidence and prevalence in the United States through 2030, J. Am. Soc. Nephrol. 30 (2019) 127–135, https://doi.org/10.1681/ASN.2018050531.
[4] United States Renal Data System, 2023 USRDS Annual Data Report: Epidemiology of kidney disease in the United States Annual Data Report, National Institutes of Health, National Institute of Diabetes and Digestive and Kidney Diseases (2023).
[5] M. Dąbrowska-Bender, G. Dykowska, W. Żuk, M. Milewska, A. Staniszewska, The impact on quality of life of dialysis patients with renal insufficiency, Patient Prefer. Adherence 12 (2018) 577–583, https://doi.org/10.2147/PPA.S156356.
[6] V. Kolarić, V. Svirčević, R. Bijuk, V. Zupančič, Chronic complications of diabetes and quality of life, Acta Clin. Croat. 61 (2022) 520–526, https://doi.org/10.20471/acc.2022.61.03.18.
[7] S.W. Jung, J.-Y. Moon, The role of inflammation in diabetic kidney disease, Korean, J. Intern. Med. 36 (2021) 753–766, https://doi.org/10.3904/kjim.2021.174.
[8] Y.-L. Chen, Y.-C. Qiao, Y. Xu, W. Ling, Y.-H. Pan, Y.-C. Huang, L.-J. Geng, H.-L. Zhao, X.-X. Zhang, Serum TNF-α concentrations in type 2 diabetes mellitus patients and diabetic nephropathy patients: a systematic review and meta-analysis, Immunol. Lett. 186 (2017) 52–58, https://doi.org/10.1016/j.imlet.2017.04.003.
[9] R. Abu Hamad, S. Berman, Y. Hachmo, M. Stark, F. Hasan, K. Doenyas-Barak, S. Efrati, Response of renal podocytes to excessive hydrostatic pressure: a pathophysiologic cascade in a malignant hypertension model, kidney blood press, Res. 42 (2017) 1104–1118, https://doi.org/10.1159/000485774.
[10] W. Kriz, B. Hähnel, H. Hosser, S. Rösener, R. Waldherr, Structural analysis of how podocytes detach from the glomerular basement membrane under hypertrophic stress, Front Endocrinol. 5 (2014).
[11] A. Chagnac, B. Zingerman, B. Rozen-Zvi, M. Herman-Edelstein, Consequences of glomerular hyperfiltration: the role of physical forces in the pathogenesis of chronic kidney disease in diabetes and obesity, Nephron 143 (2019) 38–42, https://doi.org/10.1159/000499486.
[12] M.E. Pagtalunan, P.L. Miller, S. Jumping-Eagle, R.G. Nelson, B.D. Myers, H. G. Rennke, N.S. Coplon, L. Sun, T.W. Meyer, Podocyte loss and progressive glomerular injury in type II diabetes, J. Clin. Invest. 99 (1997) 342–348.
[13] K.E. White, R.W. Bilous, S.M. Marshall, M. El Nahas, G. Remuzzi, G. Piras, S. De Cosmo, G. Viberti, on behalf of the European Study for the Prevention of Renal Disease in Type 1 Diabetes (ESPRIT), Podocyte Number in Normotensive Type 1 Diabetic Patients With Albuminuria, Diabetes 51 (2002) 3083–3089, https://doi.org/10.2337/diabetes.51.10.3083.
[14] D. Cosgrove, R. Kalluri, J.-H. Miner, Y. Segal, D.-B. Borza, Choosing a mouse model to study the molecular pathobiology of Alport glomerulonephritis, Kidney Int. 71 (2007) 615–618, https://doi.org/10.1038/sj.ki.5002115.
[15] M. Schindler, A. Blumenthal, M.J. Moeller, K. Endlich, N. Endlich, Adriamycin does not damage podocytes of zebrafish larvae, PLOS ONE 15 (2020) e0242436.
[16] T.D. Kalejaiye, R. Bhattacharya, M.A. Burt, T. Travieso, A.E. Okafor, X. Mou, M. Blasi, S. Musah, SARS-CoV-2 employ BSG/CD147 and ACE2 receptors to directly infect human induced pluripotent stem cell-derived kidney podocytes, Front. Cell Dev. Biol. 10 (2022), https://doi.org/10.3389/fcell.2022.855340.
[17] M.A. Burt, T.D. Kalejaiye, R. Bhattacharya, N. Dimitrakakis, S. Musah, Adriamycin-induced podocyte injury disrupts the YAP-TEAD1 axis and downregulates Cyr61 and CTGF expression, ACS Chem. Biol. 17 (2022) 3341–3351, https://doi.org/10.1021/acschembio.1c00678.
[18] X. Mou, J. Shah, Y. Roye, C. Du, S. Musah, An ultrathin membrane mediates tissue-specific morphogenesis and barrier function in a human kidney chip, Sci. Adv. 10 (2024) eadn2689, https://doi.org/10.1126/sciadv.adn2689.
[19] R. Bhattacharya, T. Ward, T.D. Kalejaiye, A. Mishra, S. Leeman, H. Arzaghi, J.G. Seidman, C.E. Seidman, S. Musah, Engineered human iPS cell models reveal altered podocytogenesis and glomerular capillary wall in CHD-associated SMAD2 mutations, (2024) 2024.08.02.606108. https://doi.org/10.1101/2024.08.02.606108.
[20] Y. Roye, R. Bhattacharya, X. Mou, Y. Zhou, M.A. Burt, S. Musah, A Personalized glomerulus chip engineered from stem cell-derived epithelium and vascular endothelium, Micromachines 12 (2021) 967, https://doi.org/10.3390/mi12080967.
[21] S.D. Funk, R.H. Bayer, J.H. Miner, Endothelial cell-specific collagen type IV-α3 expression does not rescue Alport syndrome in Col4a3−/− mice, Am. J. Physiol. - Ren. Physiol. 316 (2019) F830–F837, https://doi.org/10.1152/ajprenal.00556.2018.
[22] D.R. Abrahamson, P.L. St John, L. Stroganova, A. Zelenchuk, B.M. Steenhard, Laminin and type IV collagen isoform substitutions occur in temporally and spatially distinct patterns in developing kidney glomerular basement membranes, J. Histochem. Cytochem. off. J. Histochem. Soc. 61 (2013) 706–718, https://doi.org/10.1369/0022155413501677.
[23] D.R. Abrahamson, B.G. Hudson, L. Stroganova, D.-B. Borza, P.L. St John, Cellular origins of type IV collagen networks in developing glomeruli, J. Am. Soc. Nephrol. 20 (2009) 1471, https://doi.org/10.1681/ASN.2008101086.
[24] E.N. Pokidysheva, N. Redhair, O. Ailsworth, P. Page-McCaw, L. Rollins-Smith, V. S. Jamwal, Y. Ohta, H.P. Bächinger, P. Murawala, M. Flajnik, A.B. Fogo, D. Abrahamson, J.K. Hudson, S.P. Boudko, B.G. Hudson, Collagen IV of basement membranes: II. Emergence of collagen IVα345 enabled the assembly of a compact GBM as an ultrafilter in mammalian kidneys, J. Biol. Chem. 299 (2023), https://doi.org/10.1016/j.jbc.2023.105459.
[25] D. Cosgrove, S. Liu, Collagen IV diseases: a focus on the glomerular basement membrane in alport syndrome, Matrix Biol J. Int. Soc. Matrix Biol. 57–58 (2017) 45–54, https://doi.org/10.1016/j.matbio.2016.08.005.
[26] J.H. Miner, J.R. Sanes, Collagen IV alpha 3, alpha 4, and alpha 5 chains in rodent basal laminae: sequence, distribution, association with laminins, and developmental switches, J. Cell Biol. 127 (1994) 879–891, https://doi.org/10.1083/jcb.127.3.879.
[27] J.I. Maier, M. Rogg, M. Helmstädter, A. Sammarco, O. Schilling, B. Sabass, J. H. Miner, J. Dengjel, G. Walz, M. Werner, T.B. Huber, C. Schell, EPB41L5 controls podocyte extracellular matrix assembly by adhesome-dependent force transmission, Cell Rep. 34 (2021) 108883, https://doi.org/10.1016/j.celrep.2021.108883.
[28] S. Musah, A. Mammoto, T.C. Ferrante, S.S.F. Jeanty, M. Hirano-Kobayashi, T. Mammoto, K. Roberts, S. Chung, R. Novak, M. Ingram, T. Fatanat-Didar, S. Koshy, J.C. Weaver, G.M. Church, D.E. Ingber, Mature induced-pluripotent-stem-cell-derived human podocytes reconstitute kidney glomerular-capillary-wall function on a chip, Nat. Biomed. Eng. 1 (2017) 1–12, https://doi.org/10.1038/s41551-017-0069.
[29] S. Musah, N. Dimitrakakis, D.M. Camacho, G.M. Church, D.E. Ingber, Directed differentiation of human induced pluripotent stem cells into mature kidney podocytes and establishment of a Glomerulus Chip, Nat. Protoc. 13 (2018) 1662–1685, https://doi.org/10.1038/s41596-018-0007-8.
[30] M. Burt, R. Bhattachaya, A.E. Okafor, S. Musah, Guided differentiation of mature kidney podocytes from human induced pluripotent stem cells under chemically defined conditions, JoVE J. vis. Exp. (2020) e61299.
[31] S. Hussain, L. Romio, M. Saleem, P. Mathieson, M. Serrano, J. Moscat, M. Diaz-Meco, P. Scambler, A. Koziell, Nephrin deficiency activates NF-κB and promotes glomerular injury, J. Am. Soc. Nephrol. JASN 20 (2009) 1733–1743, https://doi.org/10.1681/ASN.2008111219.
[32] C.H. Chung, J. Fan, E.Y. Lee, J.S. Kang, S.J. Lee, P.E. Pyagay, C.C. Khoury, T.-K. Yeo, M.F. Khayat, A. Wang, S. Chen, Effects of tumor necrosis factor-α on podocyte expression of monocyte chemoattractant protein-1 and in diabetic nephropathy, Nephron Extra 5 (2015) 1–18, https://doi.org/10.1159/000369576.
[33] O. Foresto-Neto, A.H. Albino, S.C.A. Arias, V.D. Faustino, F.F.F. Zambom, M. A. Cenedeze, R.M. Elias, D.M.A.C. Malheiros, N.O.S. Camara, C.K. Fujihara, R. Zatz, NF-κB system is chronically activated and promotes glomerular injury in experimental type 1 diabetic kidney disease, Front. Physiol. 11 (2020) 84, https://doi.org/10.3389/fphys.2020.00084.
[34] C. Lavoz, Y.S. Matus, M. Orejudo, J.D. Carpio, A. Droguett, J. Egido, S. Mezzano, M. Ruiz-Ortega, Interleukin-17A blockade reduces albuminuria and kidney injury

in an accelerated model of diabetic nephropathy, Kidney Int. 95 (2019) 1418–1432, https://doi.org/10.1016/j.kint.2018.12.031.
[35] P. Khajehdehi, M. Pakfetrat, K. Javidnia, F. Azad, L. Malekmakan, M.H. Nasab, G. Dehghanzadeh, Oral supplementation of turmeric attenuates proteinuria, transforming growth factor-β and interleukin-8 levels in patients with overt type 2 diabetic nephropathy: a randomized, double-blind and placebo-controlled study, Scand. J. Urol. Nephrol. 45 (2011) 365–370, https://doi.org/10.3109/00365599.2011.585622.
[36] A.A. Eid, Y. Gorin, B.M. Fagg, R. Maalouf, J.L. Barnes, K. Block, H.E. Abboud, Mechanisms of podocyte injury in diabetes, Diabetes 58 (2009) 1201–1211, https://doi.org/10.2337/db08-1536.
[37] N. Mahtal, O. Lenoir, P.-L. Tharaux, Glomerular endothelial cell crosstalk with podocytes in diabetic kidney disease, Front. Med. 8 (2021) 334, https://doi.org/10.3389/fmed.2021.659013.
[38] L. Atchison, N.O. Abutaleb, E. Snyder-Mounts, Y. Gete, A. Ladha, T. Ribar, K. Cao, G.A. Truskey, iPSC-derived endothelial cells affect vascular function in a tissue-engineered blood vessel model of hutchinson-gilford progeria syndrome, Stem Cell Rep. 14 (2020) 325–337, https://doi.org/10.1016/j.stemcr.2020.01.005.
[39] Y. Roye, S. Musah, Isogenic kidney glomerulus chip engineered from human induced pluripotent stem cells, JoVE J. vis. Exp. (2022) e63821.
[40] F. Liao, H.K. Huynh, A. Eiroa, T. Greene, E. Polizzi, W.A. Muller, Migration of monocytes across endothelium and passage through extracellular matrix involve separate molecular domains of PECAM-1, J. Exp. Med. 182 (1995) 1337–1343, https://doi.org/10.1084/jem.182.5.1337.
[41] L. Wang, H.-L. Wang, T.-T. Liu, H.-Y. Lan, TGF-beta as a master regulator of diabetic nephropathy, Int. J. Mol. Sci. 22 (2021) 7881, https://doi.org/10.3390/ijms22157881.
[42] D.K. Newman, G. Fu, T. Adams, W. Cui, V. Arumugam, T. Bluemn, M.J. Riese, The adhesion molecule PECAM-1 enhances the TGF-β–mediated inhibition of T cell function, Sci. Signal. 9 (2016) ra27, https://doi.org/10.1126/scisignal.aad1242.
[43] X.R. Huang, A.C.K. Chung, X.J. Wang, K.N. Lai, H.Y. Lan, Mice overexpressing latent TGF-β1 are protected against renal fibrosis in obstructive kidney disease, Am. J. Physiol. Renal Physiol. 295 (2008) F118–F127, https://doi.org/10.1152/ajprenal.00021.2008.
[44] L.M. Russo, E. del Re, D. Brown, H.Y. Lin, Evidence for a role of transforming growth factor (TGF)-beta1 in the induction of postglomerular albuminuria in diabetic nephropathy: amelioration by soluble TGF-beta type II receptor, Diabetes 56 (2007) 380–388, https://doi.org/10.2337/db06-1018.
[45] A. Ruggiero, P. Ferrara, G. Attinà, D. Rizzo, R. Riccardi, Renal toxicity and chemotherapy in children with cancer, Br. J. Clin. Pharmacol. 83 (2017) 2605–2614, https://doi.org/10.1111/bcp.13388.
[46] Y. Ni, X. Wang, X. Yin, Y. Li, X. Liu, H. Wang, X. Liu, J. Zhang, H. Gao, B. Shi, S. Zhao, Plectin protects podocytes from adriamycin-induced apoptosis and F-actin cytoskeletal disruption through the integrin α6β4/FAK/p38 MAPK pathway, J. Cell. Mol. Med. 22 (2018) 5450–5467, https://doi.org/10.1111/jcmm.13816.
[47] V.W. Lee, D.C. Harris, Adriamycin nephropathy: a model of focal segmental glomerulosclerosis, Nephrology 16 (2011) 30–38, https://doi.org/10.1111/j.1440-1797.2010.01383.x.
[48] K.N. Campbell, J.A. Tumlin, Protecting podocytes: a key target for therapy of focal segmental glomerulosclerosis, Am. J. Nephrol. 47 (2018) 14–29, https://doi.org/10.1159/000481634.
[49] L. Blonde, P. Aschner, C. Bailey, L. Ji, L.A. Leiter, S. Matthaei, Gaps and barriers in the control of blood glucose in people with type 2 diabetes, Diab. Vasc. Dis. Res. 14 (2017) 172–183, https://doi.org/10.1177/1479164116679775.
[50] Labib A, Rosen J, Yosipovitch G. Skin Manifestations of Diabetes Mellitus. In: Feingold KR, Anawalt B, Blackman MR, Boyce A, Chrousos G, Corpas E, et al., editors. Endotext.; 2000.
[51] A.D. Mooradian, Diabetes-related perturbations in the integrity of physiologic barriers, J. Diabetes Complications 37 (2023) 108552, https://doi.org/10.1016/j.jdiacomp.2023.108552.
[52] B. Teng, P. Schroder, J. Müller-Deile, H. Schenk, L. Staggs, I. Tossidou, I. Dikic, H. Haller, M. Schiffer, CIN85 deficiency prevents nephrin endocytosis and proteinuria in diabetes, Diabetes 65 (2016) 3667–3679, https://doi.org/10.2337/db16-0081.
[53] B. Jim, M. Ghanta, A. Qipo, Y. Fan, P.Y. Chuang, H.W. Cohen, M. Abadi, D. B. Thomas, J.C. He, Dysregulated nephrin in diabetic nephropathy of type 2 diabetes: a cross sectional study, PLOS ONE 7 (2012) e36041.
[54] S. Doublier, G. Salvidio, E. Lupia, V. Ruotsalainen, D. Verzola, G. Deferrari, G. Camussi, Nephrin expression is reduced in human diabetic nephropathy: evidence for a distinct role for glycated albumin and angiotensin II, Diabetes 52 (2003) 1023–1030, https://doi.org/10.2337/diabetes.52.4.1023.
[55] I. Kostovska, K. Tosheska-Trajkovska, S. Topuzovska, S. Cekovska, G. Spasovski, O. Kostovski, D. Labudovic, Urinary nephrin is earlier, more sensitive and specific marker of diabetic nephropathy than microalbuminuria, J. Med. Biochem. 39 (2020) 83–90, https://doi.org/10.2478/jomb-2019-0026.
[56] M. Surya, M. Rajappa, Utility of urinary nephrin in patients with and without diabetic nephropathy and its correlation with albuminuria, Cureus 13 (2021) e20102.
[57] Y. Tian, X. Chen, X. Liang, X. Wu, C. Yao, SGLT2 inhibitors attenuate nephrin loss and enhance TGF-β1 secretion in type 2 diabetes patients with albuminuria: a randomized clinical trial, Sci. Rep. 12 (2022) 15695, https://doi.org/10.1038/s41598-022-19988-7.
[58] A. Levin, A. Reznichenko, A. Witasp, P. Liu, P.J. Greasley, A. Sorrentino, T. Blondal, S. Zambrano, J. Nordström, A. Bruchfeld, P. Barany, K. Ebefors, F. Erlandsson, J. Patrakka, P. Stenvinkel, J. Nyström, A. Wernerson, Novel insights into the disease transcriptome of human diabetic glomeruli and tubulointerstitium, Nephrol. Dial. Transplant. 35 (2020) 2059–2072, https://doi.org/10.1093/ndt/gfaa121.
[59] M.R. Morais, P. Tian, C. Lawless, S. Murtuza-Baker, L. Hopkinson, S. Woods, A. Mironov, D.A. Long, D.P. Gale, T.M. Zorn, S.J. Kimber, R. Zent, R. Lennon, Kidney organoids recapitulate human basement membrane assembly in health and disease, eLife 11 (2022) e73486. https://doi.org/10.7554/eLife.73486.
[60] L. Ning, H.Y. Suleiman, J.H. Miner, Synaptopodin is dispensable for normal podocyte homeostasis but is protective in the context of acute podocyte injury, J. Am. Soc. Nephrol. JASN 31 (2020) 2815–2832, https://doi.org/10.1681/ASN.2020050572.
[61] Q. Sha, J. Lyu, M. Zhao, H. Li, M. Guo, Q. Sun, Multi-omics analysis of diabetic nephropathy reveals potential new mechanisms and drug targets, Front. Genet. 11 (2020) 616435, https://doi.org/10.3389/fgene.2020.616435.
[62] S.G. Adler, S. Feld, L. Striker, G. Striker, J. Lapage, C. Esposito, J. Aboulhosn, L. Barba, D.R. Cha, C.C. Nast, Glomerular type IV collagen in patients with diabetic nephropathy with and without additional glomerular disease, Kidney Int. 57 (2000) 2084–2092.
[63] M.C. Iglesias-de la Cruz, F.N. Ziyadeh, M. Isono, M. Kouahou, D.C. Han, R. Kalluri, P. Mundel, S. Chen, Effects of high glucose and TGF-β1 on the expression of collagen IV and vascular endothelial growth factor in mouse podocytes, Kidney Int. 62 (2002) 901–913, https://doi.org/10.1046/j.1523-1755.2002.00528.x.
[64] X. Lin, J.H. Suh, G. Go, J.H. Miner, Feasibility of repairing glomerular basement membrane defects in alport syndrome, J. Am. Soc. Nephrol. 25 (2014) 687–692, https://doi.org/10.1681/ASN.2013070798.
[65] S. Conti, N. Perico, R. Novelli, C. Carrara, A. Benigni, G. Remuzzi, Early and late scanning electron microscopy findings in diabetic kidney disease, Sci. Rep. 8 (2018) 4909, https://doi.org/10.1038/s41598-018-23244-2.
[66] H. Qu, X. Gong, X. Liu, R. Zhang, Y. Wang, B. Huang, L. Zhang, H. Zheng, Y. Zheng, Deficiency of mitochondrial glycerol 3-phosphate dehydrogenase exacerbates podocyte injury and the progression of diabetic kidney disease, Diabetes 70 (2021) 1372–1387, https://doi.org/10.2337/db20-1157.
[67] V.S. LeBleu, K. Kanasaki, S. Lovisa, J.L. Alge, J. Kim, Y. Chen, Y. Teng, B. Gerami-Naini, H. Sugimoto, N. Kato, I. Revuelta, N. Grau, J.P. Sleeman, G. Taduri, A. Kizu, S. Rafii, K. Hochedlinger, S.E. Quaggin, R. Kalluri, Genetic reprogramming with stem cells regenerates glomerular epithelial podocytes in Alport syndrome, Life Sci. Alliance 7 (2024), https://doi.org/10.26508/lsa.202402664.
[68] T.D. Kalejaiye, A.D. Barreto, S. Musah, Translating organoids into artificial kidneys, Curr. Transplant. Rep. 9 (2022) 276–286, https://doi.org/10.1007/s40472-022-00383-0.
[69] J. Eyckmans, Hacking mechanical memory, Biophys. J. 122 (2023) 1423–1425, https://doi.org/10.1016/j.bpj.2023.03.012.
[70] A.K. Scott, E. Casas, S.E. Schneider, A.R. Swearingen, C.L. Van Den Elzen, B. Seelbinder, J.E. Barthold, J.F. Kugel, J.L. Stern, K.J. Foster, N.C. Emery, J. Brumbaugh, C.P. Neu, Mechanical memory stored through epigenetic remodeling reduces cell therapeutic potential, Biophys. J. 122 (2023) 1428–1444, https://doi.org/10.1016/j.bpj.2023.03.004.
[71] A. Remuzzi, M. Figliuzzi, B. Bonandrini, S. Silvani, N. Azzollini, R. Nossa, A. Benigni, G. Remuzzi, Experimental evaluation of kidney regeneration by organ scaffold recellularization, Sci. Rep. 7 (2017) 43502, https://doi.org/10.1038/srep43502.
[72] O. Ciampi, B. Bonandrini, M. Derosas, S. Conti, P. Rizzo, V. Benedetti, M. Figliuzzi, A. Remuzzi, A. Benigni, G. Remuzzi, S. Tomasoni, Engineering the vasculature of decellularized rat kidney scaffolds using human induced pluripotent stem cell-derived endothelial cells, Sci. Rep. 9 (2019) 8001, https://doi.org/10.1038/s41598-019-44393-y.
[73] J. Yu, M.A. Vodyanik, K. Smuga-Otto, J. Antosiewicz-Bourget, J.L. Frane, S. Tian, J. Nie, G.A. Jonsdottir, V. Ruotti, R. Stewart, I.I. Slukvin, J.A. Thomson, Induced pluripotent stem cell lines derived from human somatic cells, Science 318 (2007) 1917–1920, https://doi.org/10.1126/science.1151526.